Anthropomorphic, Compliant and Lightweight Dual Arm System for Aerial Manipulation

Alejandro Suarez, Pablo Ramon Soria, Guillermo Heredia, Begoña C. Arrue, Anibal Ollero

Abstract— This paper presents a low weight (1.3 kg), human size dual arm system with compliant joints designed for aerial manipulation with a multirotor platform. Each arm provides four degrees of freedom (DOF) for end effector positioning in a kinematic configuration close to the human arm: shoulder pitch, roll and yaw, and elbow pitch. The aluminum frame structure of the arms has been designed with a double purpose: protecting the servo actuators against direct impacts and overloads, and allowing the integration of a compliant transmission mechanism with deflection measurement between the servo shaft and the output link. Mechanical joint compliance increases safety in the physical interactions with the environment, removing also joint overloads typical in closed kinematic chain configurations. The dual arm system has been integrated in a hexarotor platform with a visual servoing system for object grasping, evaluating its performance first in a fixed base test bench and later in outdoor flight tests.

I. INTRODUCTION

One of the main factors that determine the performance of an aerial manipulation system is the level of dexterity of its manipulator. In this sense, it would result highly convenient to provide the aerial platform with a human-like manipulation capability, in such a way that the tasks or operations can be done in way similar a human operator would do. However, the designer should deal with payload limitations imposed by the UAV (Unmanned Aerial Vehicle), as well as motion and space constraints associated to the landing gear and the frame structure of the platform. Two approaches can be found in the development of an aerial manipulation systems: 1) integrating commercially available robotic arms, as the 7-DOF industrial manipulator mounted on an autonomous helicopter described in [1], or 2) develop robotic arms specifically designed for their integration in aerial platforms. Several prototypes and medium TRL (technological readiness level) products have been developed, either 2-DOF with shoulder pitch and elbow pitch joints [2], 5-DOF [3] or 6-DOF [4]. A quadrotor with two 2-DOF manipulators is employed in [5] for valve turning operation, whereas the dual arm manipulator presented in [6] is applied for object transportation.

If the aerial manipulator is expected to execute operations or tasks involving physical interactions with the environment on flight, such as grasping [7][8], peg-in-hole or assembly [9], then it is necessary to prevent that the contact forces are rigidly propagated through the manipulator, from end effector to the base of the UAV. Mechanical joint compliance has been introduced in the design of lightweight robotic arms in several works. Ref. [10] exploits the deflection of the elbow joint for

A. Suarez (asuarezfm@us.es), P. Ramon-Soria (pabramsor@gmail.com), G. Heredia (guiller@us.es), B. C. Arrue (barrue@us.es) and A. Ollero (aollero@us.es) are with the Robotics, Vision and Control Group at the University of Seville, Spain.

estimating the weight of the grabbed object and for active energy release after a collision happens. Obstacle localization, soft-collision detection and reaction, and contact force control capabilities are demonstrated with the 3-DOF compliant and lightweight arm prototype presented in [11]. A compliant element is used in [12] for storing the energy generated during the impact of an aerial manipulator. The analysis of a flexible single joint arm mounted on a quadrotor interacting with the environment can be found in [13].

This paper presents the first anthropomorphic, compliant and lightweight (1.3 kg) dual arm system designed for aerial manipulation with multirotor platform, showing its application to object grasping in test bench and in outdoors flight tests (Figure 1). The paper describes the mechanical construction of the arms, paying special attention to the design of the frame structure manufactured in aluminum, in such a way that the servo actuators are protected against impacts and radial/axial overloads. A compact spring-lever transmission mechanism is introduced in all joints for providing compliance. This feature improves the protection of the manipulator and the platform against impacts and contact forces during grasping operations. A control method based on inverse kinematics is applied to a visual servoing task, generating smooth trajectories from the Tool Center Point (TCP) to the grasping points given by the vision based object detection algorithm described in [18]. This algorithm learns the object offline to be able to detect and locate it latterly. The benefits of mechanical joint compliance are evidenced in a manual guidance experiment with the arms grasping an object forming a closed kinematic chain. The manual operation of the arms with a 6-DOF mouse is also evaluated for object grasping and release operations.
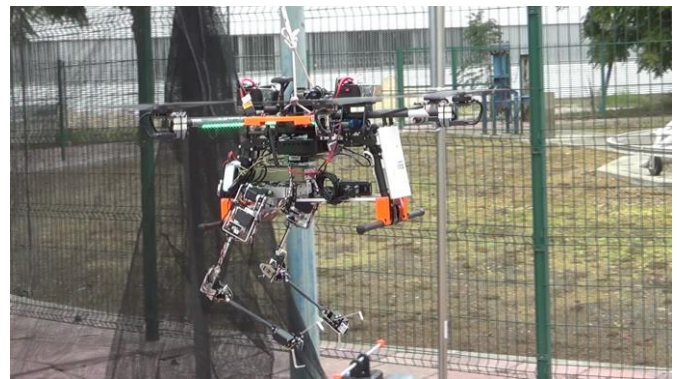

Figure 1. Aerial manipulation system consisting of the anthropomorphic compliant dual arm manipulator integrated in a hexarotor platform. The rope above the UAV was used for safety but did not have a significant influence in the dynamic behavior.

The rest of the paper is organized as follows. Section II describes the developed dual arm prototype, including some design considerations related to aerial manipulation, the frame structure and the mechanical specifications, the integration in

a hexarotor platform, and the hardware/software architecture. Section III covers the kinematic and dynamic modeling, along with the control method based on inverse kinematics for visual servoing. Section IV describes the vision algorithm employed for detecting and localizing the object to grasp. The results of this work are shown in Section V, whereas Section VI presents the conclusions.

II. ANTHROPOMORPHIC DUAL ARM SYSTEM

A. Design Considerations

The design and development of robotic arms intended to aerial manipulation applications is still a hard task due to the strong requirements imposed by this kind of platforms in terms of low weight and inertia, mechanical robustness and high dexterity, as well as the typical motion constraints and space limitations associated to the landing gear and the frame structure. Nowadays, a medium scale multirotor platform (~5 kg weight) commercially available provides 15 – 20 minutes of flight time with payloads around 2 kg. In practice, it results convenient that the total weight of the manipulator does not exceed half the maximum payload of the UAV, so the motors of the propellers are not damaged due to overload.

Smart servos like Herkulex or Dynamixel are commonly employed for building low weight and low cost robotic arms due to their high torque to weight ratio, simple assembly and because they provide relatively good features in terms of feedback and control. However these servos present important technological limitations, mainly associated to the lack of acceleration/torque feedback, as well as low update rates (<100 Hz). In order to cope with these limitations, it results convenient to introduce a compliant transmission mechanism, based for example on compression springs, between the servo shaft and the output link. The joint torque can be estimated from the deflection of the springs, what can be measured with potentiometers or encoders without the need of strain gauges. On the other hand, the compliant element will absorb the energy of impacts and overloads in a passive way at higher rates, allowing active energy release at lower rates. This increases safety in those operations involving contact forces with the environment. Mechanical joint compliance results especially useful when the arms should grasp and move an object in a coordinated way, as torque overloads associated to the closed kinematic chain can be supported by the elastic element, typically steel springs.

The design of the frame parts and structure is typically the most complicated task as it is related with the manufacturing process, materials and components available. Aluminum is a convenient material due to its low weight, low cost and high impact resistance. Take as reference that the mass density of the aluminum (frame), steel (nuts, screws) and plastic (flange bearings) is 2.75, 8.75 and 1.4 g/cm^3, respectively.

B. Dual Arm System Design

A picture of the developed anthropomorphic, compliant and lightweight dual arm prototype can be seen in Figure 2. The manipulator consists of a shoulder frame structure that supports the shoulder pitch servos (base) and the electronics, and two identical arms, left and right, equipped with a gripper. Each arm provides 4 DOF for end-effector positioning in a human-like kinematic configuration: shoulder pitch, roll and

yaw, and elbow pitch joint. The wrist orientation mechanism has not been implemented in this version.
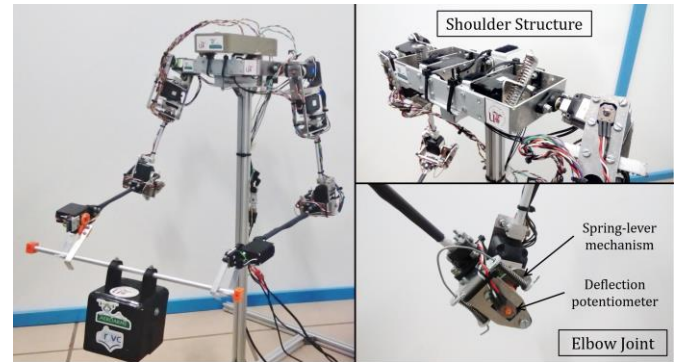

Figure 2. Prototype of anthropomorphic, compliant and lightweight dual arm system designed for aerial manipulation.

The main specifications of the dual arm system and its joints are summarized in Table 1 and Table 2, respectively. A spring-lever transmission mechanism has been included in all the joints for providing compliance. This mechanism prevents that the internal protection method of the Herkulex servos, based on temperature or PWM monitoring, is activated due to overload. A Murata SV01A potentiometer is integrated in the joints for measuring the deflection, although they are not used in this work. Eighteen igus® EFOM-08 and EFSM-06 flange bearings are employed for supporting the links, isolating the servos from direct radial/axial loads and impacts, allowing the deflection of the output link w.r.t. the servo shaft too.

Table 1. Specifications of the anthropomorphic, compliant dual arm

Weight [kg]	1.3
Max. lift load [kg]	~0.3 (per arm)
Dimensions [cm]	Forearm, Upper arm length: 25
	Separation between arms: 32
Rotation range [deg]	±90, [-30, 90], ±90, ±120
Joint deflection [deg]	~20 (maximum)

Table 2. Specifications of the compliant joints

Joint	Herkulex servo	Torque / Speed [kg·cm / rpm]	Spring constant [N/mm]	Spring length [mm]	Lever length [mm]
Shoulder pitch	DRS-0201	24 / 60	3.26	30.5	30
Shoulder roll	DRS-0201	24 / 60	2.33	28.5	30
Shoulder yaw	DRS-0101	12 / 60	2	20	20
Elbow pitch	DRS-0101	12 / 60	3.52	28	20

C. Integration in Aerial Platform

The dual arm prototype has been integrated in a hexarotor platform manufactured by *DroneTools*. The arms are endowed under the central hub, between the legs of the landing gear. This ensures that the center of mass of the aerial manipulator is aligned, and the workspace of the arms is not constrained by

the landing gear. Figure 3 shows a rendered view of the aerial manipulator. Note that the shoulder roll joint of the arms becomes especially useful when the platform is landed. The total weight of the system is 6.8 kg, with 15 min flight time.

Figure 3. 3D view of the arms integrated in the hexarotor platform between the legs of the landing gear. A ZED camera provides 120 deg FoV (green).

D. Hardware/Software Architecture

The aerial manipulation system consists of the hexarotor platform with the PX4 autopilot, the dual arm prototype, an Intel NUC computer for onboard processing, a ZED stereo camera, and a 5.8 GHz link for controlling the system from a ground control station. The different components and software modules related to the manipulator are depicted in Figure 4. All the software is developed in C/C++, running in Ubuntu 14.04, using the OpenCV 3.0 library for image processing. The task manager gets information from the different threads (servos, vision, teleoperation and STM32 micro controller board), executing the task indicated by the operation code sent by the operator. The visual servoing and manual operation controllers are implemented here along with other low level tasks. The left/right arm controllers keep updated the state of the joints, taking care of the fordward/inverse kinematics. The vision module detailed in Section IV provides visual feedback to the ground control station (GCS) and the grasping points to the visual servoing controller. The hexarotor is controlled with a standard autopilot without any feedback from the dual arm system for validating the lightweight and low inertia design.
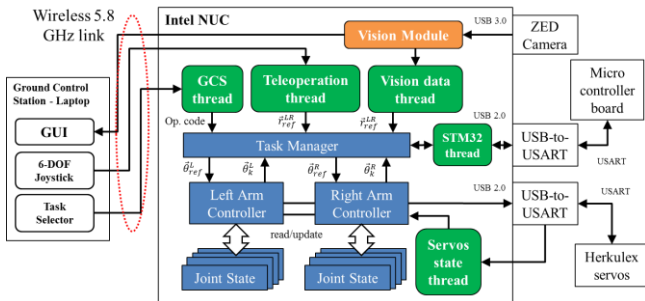

Figure 4. Hardware/software architecture of the dual arm aerial manipulator.

III. MODELING AND CONTROL

A. Kinematic Model

The developed dual arm manipulator provides 4 DOF per arm for end effector positioning. The current prototype does not include the wrist orientation mechanism. The proposed human-like kinematic configuration consists of the shoulder pitch joint at the base, followed by the shoulder roll and yaw joints, and the elbow pitch joint. Figure 5 represents the joint variables, dimensions, and vectors associated to the kinematic model. Here q_j^i represents the angular position of the j-th joint

of the i-th arm, with $i = \{1, 2\}$ for the left and right arms, and $j = \{1, 2, 3, 4\}$ for the shoulder pitch, roll, yaw and elbow pitch joints. L_1 and L_2 are the upper arm link and forearm link lengths, respectively, D is the separation between the arms, whereas r^i, r^i_{ref} and $e^i \in \mathbb{R}^3$ are the Cartesian position of the TCP, the reference grasping point, and the positioning error.
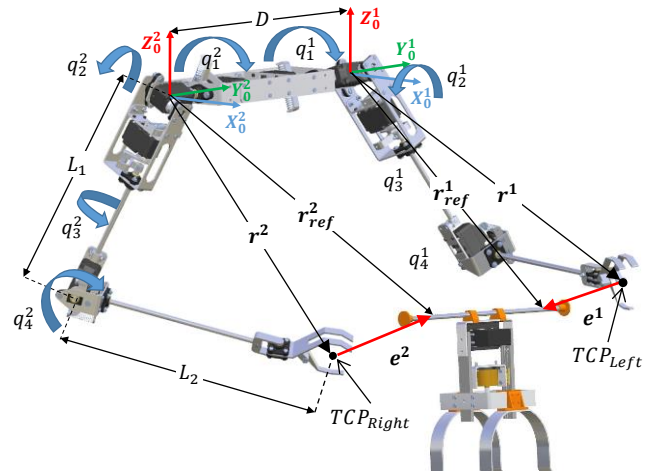

Figure 5. Kinematic model of the anthropomorphic dual arm system. The object to be grasped is an inspection tool installable on pipe.

Let us define the coordinate system associated to the base of the i-th arm as $\{i, 0\}$, while $\{i, j\}$ represents the coordinate system of each link, with the sign criteria indicated in Figure 5. Denoting by $^iT_j^{j-1} \in \mathbb{R}^{4 \times 4}$ to the transformation matrix of the j-link of the i-th arm, the position of the TCP is computed applying the forward kinematic model:

$$r^i = \begin{bmatrix} x^i \\ y^i \\ z^i \end{bmatrix} = F_i(q^i) = \left(\prod_{j=1}^{4} T_j^{j-1}(q_j^i) \right) \begin{bmatrix} 0 \\ 0 \\ -L_2 \\ 1 \end{bmatrix} \quad (1)$$

Here L_2 represents the distance from the elbow joint to the TCP. Although the definition of the transformation matrices is omitted for space limitations, it is necessary to remark that T_4^3 will depend on the upper arm link length, L_1. Note also that the proposed kinematic configuration provides one redundant degree of freedom that can be exploited in several ways: null space control, collision avoidance, or end effector orientation. The shoulder roll joint is mainly used for lifting the forearm to a plane above the landing gear in order to avoid the collision with the floor in the take-off and landing operations. In the visual servoing task, it is imposed that $q_2^i = \phi^i$ for simplicity, where the swivel angle ϕ^i is adjusted to a fixed value that depends on the workspace.

In the inverse kinematic model, given a Cartesian point of the TCP, the position of the joints are obtained:

$$q^i = F_i^{-1}(r^i) = \Omega_i(r^i) \quad (2)$$

The elbow pitch angle has immediate analytical solution:

$$q_4^i = -\cos^{-1}\left(\frac{x_i^2 + y_i^2 + z_i^2 - L_1^2 - L_2^2}{2 \cdot L_1 \cdot L_2} \right) \quad (3)$$

The shoulder pitch angle satisfies the following equation, whose analytical solution is omitted:

$$x^i \cdot sin(q_1^i) + z^i \cdot cos(q_1^i) = w_i \qquad (4)$$

where w_i is defined as follows:

$$w_i = \frac{L_2^2 - (L_1^2 + x_i^2 + z_i^2) + 2 \cdot L_1 \cdot y_i \cdot sin(q_2^i)}{2 \cdot L_1 \cdot cos(q_2^i)} \qquad (5)$$

Finally, the shoulder yaw angle is obtained as follows:

$$q_3^i = atan2(a^i, b^i) \qquad (6)$$
$$a^i = x_i s(q_1^i)s(q_2^i) + y_i c(q_2^i) + z_i c(q_1^i)s(q_2^i) \qquad (7)$$
$$b^i = x_i c(q_1^i) - z_i s(q_1^i) \qquad (8)$$

Here $s(\alpha) = \sin(\alpha)$ and $c(\beta) = \cos(\beta)$.

B. Dynamic Model

This subsection introduces the dynamics of the compliant joint dual arm manipulator [14], which can be extended to the closed kinematic chain case [15]. The dynamic model of the whole dual arm aerial manipulation system is out of the scope of this work, although references [16] [17] can be followed. Let θ_j^i denote the angular position of the servo shaft in the j-th joint of the i-th arm, whereas q_j^i is the angular position of the output link. The deflection angle of the compliant joint, represented as $\Delta\theta_j^i$, is then defined as follows:

$$\Delta\theta_j^i = q_j^i - \theta_j^i \qquad (9)$$

Considering a spring-damper dynamic model, the torque generated by the compliant transmission will be:

$$\tau_j^i = k_j^i \cdot \Delta\theta_j^i + d_j^i \cdot (\dot{q}_j^i - \dot{\theta}_j^i) \qquad (10)$$

where k_j^i and d_j^i are the elastic and friction constants. The dynamic equations for each manipulator are decomposed in two parts, the servo dynamics and the output link dynamics, related by the transmitted torque $\boldsymbol{\tau}^i \epsilon \mathbb{R}^4$:

$$\boldsymbol{B}_i(\boldsymbol{\theta}^i)\ddot{\boldsymbol{\theta}}^i + \boldsymbol{\tau}^i = \boldsymbol{\tau}_m^i - \boldsymbol{\tau}_f^i \qquad (11)$$

$$\boldsymbol{M}_i(\boldsymbol{q}^i)\ddot{\boldsymbol{q}}^i + \boldsymbol{C}_i(\boldsymbol{q}^i, \dot{\boldsymbol{q}}^i) + \boldsymbol{G}_i(\boldsymbol{q}^i) = \boldsymbol{\tau}^i + \boldsymbol{\tau}_{ext}^i \qquad (12)$$

In these equations, $\boldsymbol{B}_i$ and $\boldsymbol{M}_i \epsilon \mathbb{R}^{4 \times 4}$ are the servo shaft and output link inertia matrices, $\boldsymbol{C}_i$ and $\boldsymbol{G}_i \epsilon \mathbb{R}^4$ are the Coriolis and gravity terms, and $\boldsymbol{\tau}_m^i$, $\boldsymbol{\tau}_f^i$ and $\boldsymbol{\tau}_{ext}^i \epsilon \mathbb{R}^4$ are the motor, friction and external joint torques of the i-th arm. The model can be simplified taking into account that the inertia of the servos shaft is almost negligible with respect to the output links, and imposing smooth motion for the arms, the inertia and Coriolis terms can be also neglected.

C. TCP Position Reference for Object Grasping

This subsection describes the control method implemented for object grasping. The proposed method takes into account the limitations of the Herkulex servos used in all the joints, as these actuators take as input references the goal position and the desired time for reaching it, namely the playtime. In order to achieve smooth motions, the position/play time references should be sent at the midpoint of the trapezoidal velocity profile that the servo controller generates internally.

According to Figure 5, the Cartesian positioning error for the i-th arm is defined as the difference between the grasping point given by the vision system and the TCP position that is obtained applying the direct kinematic model over the joints

position provided by the servos, $\boldsymbol{e}^i = \boldsymbol{r}_{ref}^i - \boldsymbol{r}^i$. Let call v to the desired Cartesian speed of the TCP, and T to the control period. The idea is that, in each iteration of the control loop, the TCP moves a step towards the grasping point, that is, in the direction of the normalized error vector:

$$\boldsymbol{r}_{goal}^i = \boldsymbol{r}^i + v \cdot T \cdot \frac{\boldsymbol{e}^i}{\|\boldsymbol{e}^i\|} + \Delta\boldsymbol{r}_G^i \qquad (13)$$

The terms in the right side of Equation (13) are the current position of the TCP, the increment to apply for approaching to the grasping point, and the estimated Cartesian deflection due to gravity. It is imposed that the TCP approaches to the grasping point at constant speed until the error threshold e_{th}^i is reached, decreasing then proportionally with the error:

$$v = \begin{cases} 0.2 \, [m/s] \;\; if \;\; \|\boldsymbol{e}^i\| \geq e_{th}^i = 0.04 \, [m] \\ 0.2 \cdot \frac{\|\boldsymbol{e}^i\|}{e_{th}^i} \, \left[\frac{m}{s}\right] \; if \; \|\boldsymbol{e}^i\| < e_{th}^i = 0.04 \, [m] \end{cases} \qquad (14)$$

The reference position for each servo is finally obtained applying the inverse kinematic model:

$$\boldsymbol{\theta}_{ref}^i = \Omega_i(\boldsymbol{r}_{goal}^i, \phi^i) \qquad (15)$$

IV. VISUAL SERVOING ALGORITHM

Authors, in [18], developed a vision system for object detection and location that was used for grasping objects with a single arm and a stereo camera. The algorithm consists of two stages. Firstly, a model of the object to be grasped is learned. A feature detector and descriptor is used for extracting features in a set of images taken around the object. Then its shape is reconstructed and optimized using Bundle Adjustment [19]. Finally, this feature-based model is used for the online detection of the object in new scenes. The algorithm was proven to be robust to occlusion, as shown in Figure 6, so pose can be reconstructed with partial of the features. This fact is very convenient for manipulation, as the manipulator can partially occlude the aimed object. In this work, the algorithm was speeded up using only a single camera for the online detection, running up to 20 FPS.
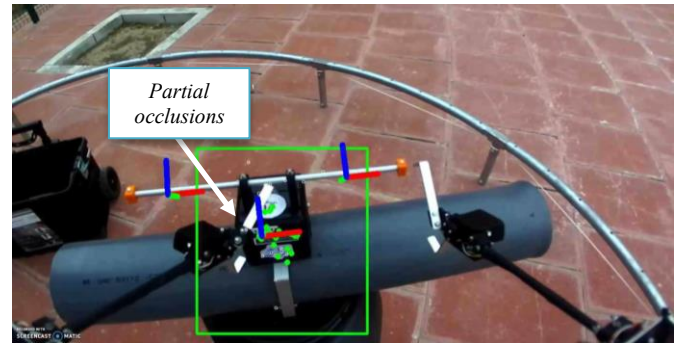

Figure 6. Coordinate system and grasping points associated to the inspection tool provided by the vision algorithm during a flight experiment.

As described in [18], the particular selection of the pair detector-descriptor is not relevant for the pipeline of the algorithm. Nevertheless, for this work, it was chosen the pair FAST-SIFT. FAST detector are computed quicker and SIFT descriptors are more robust to changes in scale, i.e. it works

better at both small and large distances. In the bimanual grasping task illustrated in Figure 6, two grasping points are generated associated to the two handles of the object. This information is sent to the control method described in Section III-C to move the arms towards the object.

In order to detect that the robot reached the grasping points, the end effectors is equipped with push buttons. In order to avoid failures, if only one push button is pushed, the whole algorithm restart the operation, opening the closed hand and returning to the approaching position.

V. EXPERIMENTAL RESULTS

A. Manual Operation

A 6-DOF mouse from *3DConnexion* has been employed for evaluating the manual operation of the arms in the object grasping and release tasks. Several experiments have been conducted in two observation conditions: direct sight at short distance between the operator and the arms ($\sim$5 m), and monocular visual feedback displayed at the GCS [20].

The 6-DOF mouse replaces the vision module, generating position references of the TCP in an incremental way. The operator acts over the joystick for controlling the normalized translational velocity on each axis, Δ_x, Δ_y and $\Delta_z \in [-1, 1]$. If $v_{max} = 0.2 \, [m/s]$ is the maximum desired Cartesian speed for the TCP, with a control period $T = 0.1 \, s$, the reference position for each iteration is then computed as follows:

$$r_{ref}^i = r^i + \begin{bmatrix} \Delta_x \\ \Delta_x \\ \Delta_x \end{bmatrix} \cdot v_{max} \cdot T \qquad (16)$$

Figure 7 shows the 3D trajectories of the left and right arms during the object grasping and release experiment using the 6-DOF mouse for manual operation, displaying the video stream from the onboard camera on a tablet (see video). The orientation DOF's provided by the mouse can be introduced in a similar way for generating different poses with the arms.
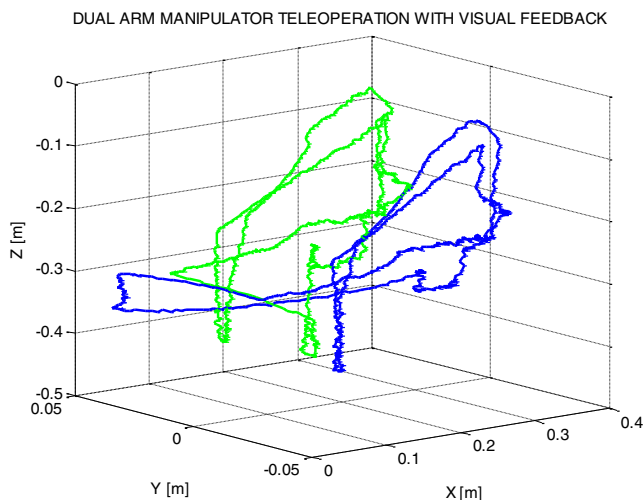

Figure 7. 3D trajectory of the left (blue) and right (green) arms in the manual teleoperation with visual feedback (around 100 ms delay).

B. Visual Servoing in Test-bench

The control method described in Section III-C has been applied for grasping the inspection tool depicted in Figure 5. The vision module presented in Section IV provides the XYZ grasping points to the controller (the Task Manager module

in Figure 4). Figure 8 shows the trajectories and references of the left and right arms, referred to their respective frames, when they move from the initial points at $[0, \pm 0.04, -0.36]^T$ to the corresponding grasping points at $[0.3, \mp 0.02, -0.3]^T$.
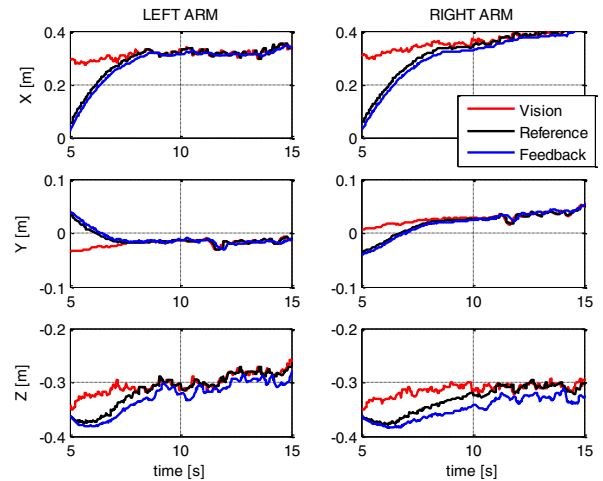

Figure 8. TCP position of the left/right arms in the grasping trajectory from the initial position. The object is grasped around t = 10 seconds.

As mentioned previously, the mechanical joint compliance provides to the aerial manipulator a certain level of tolerance against external forces and overloads that typically arise in closed kinematic chains or in operations involving physical interactions with the environment. This property has been evaluated through an experiment in which both arms grasp the inspection tool, maintaining active the visual servoing controller, while a human operator guided manually the tool. Figure 9 shows the XYZ trajectories for the left arm, that is, the grasping points given by the vision algorithm (red), the position reference generated by the controller (black) and the current position of the TCP (blue). As it can be seen, the arms follow the motion of the grasped tool while it is guided by the human. The idea is that when the operator pushes the tool, the joints are deflected, which causes a displacement of the grasping point. As long as the visual servoing controller is active, the arms will tend to go to the new grasping point.

C. Outdoor Flight Tests

Object grasping and transportation tests were conducted in outdoors with the aerial manipulator shown in Figure 1 flying in a 4 m Ø, 3 m height circular area partially covered by a security net and rope. The multirotor was controlled in position by a human pilot, with the visual servoing system running in the onboard computer. The experiment is executed in six phases: 1) approach to the inspection tool installed in the pipe, 2) visual servoing, 3) close grippers, object retrieve, 4) manual operation, 5) go to tool bench, and 6) tool release. A sequence of images from the video corresponding to this experiment can be seen in Figure 10. The object to grasp was an inspection tool with two handles attached to a pipe. It was found during the realization of the experiments that the aerial platform was not significantly affected by the motion of the arms or by contact forces despite no feedback was provided to the autopilot. This is so due to the mechanical properties of the dual arm. A video of the experiment can be found in [20].

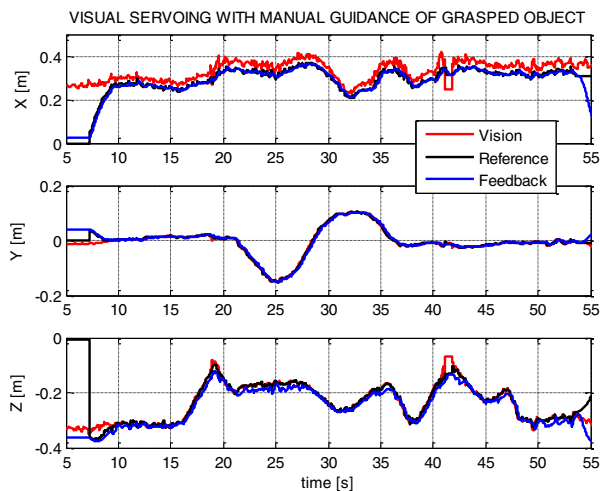VISUAL SERVOING WITH MANUAL GUIDANCE OF GRASPED OBJECT

Figure 9. Tool center point position of the left arm in the visual servoing experiment with manual object guidance while grasping.
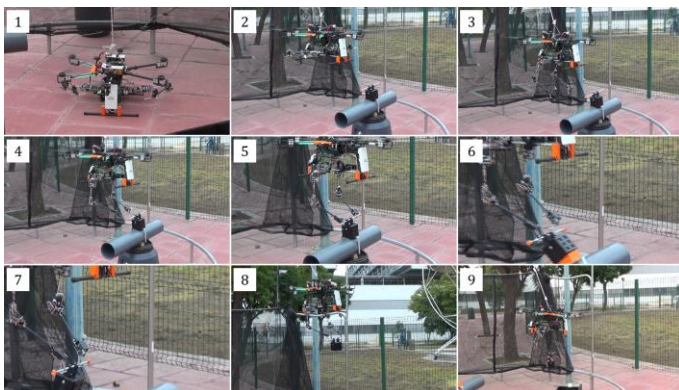

Figure 10. Sequence of images during the bimanual grasping experiment flying in outdoors: take-off (1), approaching to object (2), grasping with visual servoing (3-7) and manual operation for object release (8, 9). The safety rope above the multirotor does not significantly disturb the flight.

VI. CONCLUSION

This paper has presented an aerial manipulation system consisting of a hexarotor platform with an anthropomorphic, compliant and lightweight dual arm prototype, and the vision system for object detection and location applied to visual servoing. The proposed design, the kinematic and dynamic models, and the visual servoing method for object grasping were described. Experiments in test bench and outdoor flight tests validate the performance of the arms and the vision system, which provides the grasping points of a two-handle tool even when the object to grasp is partially occluded by the dual arm manipulator. The benefits of mechanical joint compliance have been evidenced in the guidance experiment, in which both arms form a closed kinematic chain with the grasped object while the visual servoing control is running, so the arms will follow the motions exerted by an operator.

REFERENCES

[1] Kondak, K., Huber, F., Schwarzbach, M., Laiacker, M., Sommer, D., Bejar, M., & Ollero, A. Aerial manipulation robot composed of an autonomous helicopter and a 7 DoF industrial manipulator. In Robotics and Automation (ICRA), 2014 IEEE Int. Conf on (pp. 2107-2112).

[2] Kim, S., Choi, S., & Kim, H. J. Aerial manipulation using a quadrotor with a two dof robotic arm. In Intelligent Robots and Systems (IROS), 2013 IEEE/RSJ International Conference on (pp. 4990-4995).

[3] Bellicoso, C. D., Buonocore, L. R., Lippiello, V., & Siciliano, B. (2015, June). Design, modeling and control of a 5-DoF light-weight robot arm for aerial manipulation. In Control and Automation (MED), 2015 23th Mediterranean Conference on (pp. 853-858). IEEE.

[4] Cano, R., Pérez, C., Pruano, F., Ollero, A., & Heredia, G. (2013). Mechanical design of a 6-DOF aerial manipulator for assembling bar structures using UAVs. In 2nd RED-UAS 2013 Workshop on Research, Education and Development of Unmanned Aerial Systems.

[5] Korpela, C., Orsag, M., & Oh, P.. Towards valve turning using a dual-arm aerial manipulator. In Intelligent Robots and Systems (IROS 2014), 2014 IEEE/RSJ International Conference on (pp. 3411-3416).

[6] https://www.prodrone.jp/en/archives/1420/

[7] Mellinger, D., Lindsey, Q., Shomin, M., & Kumar, V. (2011, September). Design, modeling, estimation and control for aerial grasping and manipulation. In Intelligent Robots and Systems (IROS), 2011 IEEE/RSJ International Conference on (pp. 2668-2673). IEEE.

[8] Pounds, P. E., Bersak, D. R., & Dollar, A. M. (2011, May). The yale aerial manipulator: grasping in flight. In Robotics and Automation (ICRA), 2011 International Conference on (pp. 2974-2975). IEEE.

[9] Jimenez-Cano, A. E., Martin, J., Heredia, G., Ollero, A., & Cano, R. (2013). Control of an aerial robot with multi-link arm for assembly tasks. In Robotics and Automation (ICRA), 2013 IEEE International Conference on (pp. 4916-4921).

[10] Suarez, A., Heredia, G., & Ollero, A. Lightweight compliant arm for aerial manipulation. In Intelligent Robots and Systems (IROS), 2015 IEEE/RSJ International Conference on (pp. 1627-1632).

[11] Suarez, A., Heredia, G., & Ollero, A. Lightweight compliant arm with compliant finger for aerial manipulation and grasping. In Intelligent Robots and Systems (IROS), 2016 IEEE/RSJ International Conf. on.

[12] Bartelds, T., Capra, A., Hamaza, S., Stramigioli, S., & Fumagalli, M. (2016). Compliant aerial manipulators: Toward a new generation of aerial robotic workers. *IEEE RAL*, *1*(1), 477-483.

[13] Yüksel, B., Mahboubi, S., Secchi, C., Bülthoff, H. H., & Franchi, A. (2015, May). Design, identification and experimental testing of a light-weight flexible-joint arm for aerial physical interaction. In *Robotics and Automation (ICRA), 2015 IEEE Int. Conf. on* (pp. 870-876). IEEE.

[14] Albu-Schäffer, A., Ott, C., & Hirzinger, G. (2007). A unified passivity-based control framework for position, torque and impedance control of flexible joint robots. The International Journal of Robotics Research, 26(1), 23-39.

[15] Yan, L., Mu, Z., Xu, W., & Yang, B. (2016, October). Coordinated compliance control of dual-arm robot for payload manipulation: Master-slave and shared force control. In Intelligent Robots and Systems (IROS), 2016 IEEE/RSJ Int. Conference on (pp. 2697-2702).

[16] E. Papadopoulos and A. Moosavian. Dynamics and control of space free-flyers with multiple manipulators. Advanced robotics 9.6 1994, pp. 603-624.

[17] Simetti, E., & Casalino, G. (2015). Whole body control of a dual arm underwater vehicle manipulator system. Annual Reviews in Control, 40, 191-200.

[18] Ramon Soria, P., Arrue, B.C., Ollero, A. Detection, location and grasping objects using a stereo sensor on UAV in outdoor environments. Sensors 2017, 17, 103.

[19] Triggs B., McLauchlan P.F., Hartley R.I., Fitzgibbon A.W. Bundle adjustment, a modern synthesis. In: Triggs B., Zisserman A., Szeliski R. (eds) Vision Algorithms: Theory and Practice. IWVA 1999. Lecture Notes in Computer Science, vol 1883. Springer, Berlin, Heidelberg.

[20] Video: https://www.youtube.com/watch?v=5g5DFZB42fg